

Crackling to periodic dynamics in sheared granular media

Aghil Abed Zadeh,^{1,*} Jonathan Barés,^{1,2,†} and Robert P. Behringer¹

¹*Department of Physics & Center for Non-linear and Complex Systems, Duke University, Durham, NC, USA*

²*Laboratoire de Mécanique et Génie Civil, Université de Montpellier, CNRS, Montpellier, France*

(Dated: December 3, 2024)

The local and global dynamics of a sheared granular medium are studied in a model experiment as a function of several macroscopic parameters. We observe that by changing the shear rate or the loading stiffness, the system crackles, with intermittent slip avalanches, or exhibits periodic motion. By analyzing the global force, induced while shearing, we capture the transition from the crackling to the periodic regime and associated scaling laws. We deduce a novel dynamic phase diagram as a function of the shear rate and the system's stiffness. Using photo-elasticimetry, we also capture the grain-scale stress evolution, and investigate the microscopic behavior in the different regimes.

PACS numbers: 45.70.-n 91.30.pa 62.20.F 45.70.Ht

Keywords: crackling dynamics, periodic dynamics, sheared granular medium, earthquake, photoelasticity, stick-slip

Sheared amorphous materials, like many other physical systems, yield and flow, when sufficiently loaded [1–3]. The flow can be spatially heterogeneous and intermittent in time. This intermittent behavior has been observed in many phenomena as diverse as seismicity [4, 5], fracture [6–8], damage [9, 10], friction [11, 12], plasticity [13, 14], magnetization [15, 16], wetting [17, 18], neural activity [19, 20] and granular avalanches [21–25].

In the case of granular media, it has been shown that an erratic intermittent dynamics, also called ‘crackling’ [26], is associated with the transition between jammed and unjammed states [25, 27] around the yielding point: when slowly sheared, a granular system may stick and then slip, with slip sizes that span a wide range of scales [28–31]. On the other hand, under certain conditions, some sheared systems do not obey this intermittent crackling behavior. Instead, slips occur periodically with a narrow size distribution [32–35]. For other systems, the oscillations may be damped and the granular medium flows smoothly. In addition to important safety and industrial challenges to control these dynamics, understanding the physics of these different behaviors and their transition is an important question for granular physics. And, many other associated fields exhibiting similar dynamics.

The crackling response of granular media [2, 25, 36] and the effect of the system's parameters on the dynamics, their scaling laws and avalanche shapes have been investigated [37–39]. Other studies concentrated on understanding the transition between the periodic stick-slip and steady sliding regimes [35, 40]. However, transitions from crackling dynamics have by and large not been studied. Consequently, several fundamental issues remain: Do crackling and periodic systems differ fundamentally, i.e. at a microscopic scale, or do they occur as bifurcations controlled by macroscopic control parameters? If the latter applies, how do the macroscopic parameters affect the driven system, at the global and grain scales?

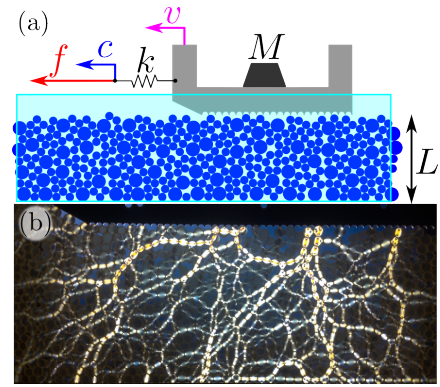


FIG. 1. (color online) (a) Schematic of the experimental setup from the side: A toothed plate of mass M is pulled over a 2D vertical granular bed of bi-disperse photoelastic discs of height $L = 9.5$ cm. The slider is pulled at a constant speed c by mean of a spring of stiffness k . The granular medium and the slider are sandwiched between two glass plates. The pulling force, f , is measured by a force sensor, connected to the spring. The system is lit from behind by polarized light and observed from the front by a fast (~ 120 fps) camera equipped with a crossed polarizer. A second camera simultaneously records the particles without a crossed polarizer. (b) Photoelastic response of the granular bed during loading.

The study reported here addresses these questions. Experiments on sheared granular materials reproduce both crackling and periodic regimes. Adjusting the driving rate, c , and the system stiffness, k , causes the system to transition from one behavior to another, and yields a dynamic phase diagram. The system observables, such as loading force f , are analyzed in both regimes. We find that microscopic stress dynamics and applied global force are not equivalent in capturing the transition.

Experiments – The experiments used an apparatus that provides data both at the global and local scales, similar to [35, 41]. As shown in fig.1(a) [42], a stage pulls a 2D frictional slider of fixed length 25 cm and variable mass

M . The stage, which moves with a constant speed c , pulls the slider through a linear spring of tunable stiffness k . The stage speed determines the average shear rate of the granular bed. The slider rests on a vertical bed of fixed depth $L = 9.5$ cm, and length 1.5 m consisting of bi-disperse cylindrical photoelastic particles with diameters 0.4 cm and 0.5 cm (small/big ratio of 2.7) to avoid crystallization. Unless specified, the experiments are made with a slider of mass $M = 85$ g. The slider+particles system is sandwiched between two dry-lubricated glass plates. The slider bottom is toothed to enhance the friction with the grains. The force, f , applied to the spring, is measured by a sensor at a frequency of 1 kHz. This force signal provides a global measure of the shear stress, τ . The system is designed to be at constant pressure, and the slider can move in either the horizontal or vertical directions. However, the granular bed is prepared flat enough that it stays mostly horizontal during an experiment. The system is lit from behind by a polarized light source. In the front, a camera with a crossed polarizer images the grains and the slider at a frequency of 120 Hz (see fig.1(b)). The photoelastic response of the media provides a local measure of the stress from the image intensity I [28]. A second camera, without a crossed polarizer, records a direct view of the system.

Results – Fig.2 shows the evolution of the pulling force, $f(t)$ (colored), and of the slider speed $v(t)$ (black), for three typical pulling speeds. At low loading speed (a) $c = 0.1$ mm/s, the system crackles [26, 41]. The slider is immobile most of the time, as it loads up slowly and elastically. It then undergoes intermittent sudden downward jumps of high intensity. These unloading events are accompanied by slipping of the slider and irreversible flows of grains. At high loading speed (c) $c = 100$ mm/s, the slider never stops, and exhibits smooth periodic oscillations. In between (b) $c = 15$ mm/s, most of the time, the slider exhibits very low speed noisy displacements with erratic jumps that are smoother and less intense than in the crackling case. Fig.2(d) shows the power spectral density (PSD) of the force signal \mathcal{P}_f for these three different cases. In the low shear rate case, above a flat lower cut-off, \mathcal{P}_f follows a power-law spanning more than two decades in ω with exponent -2.4 ± 0.2 , similar to Brownian noise [43]. At a medium c , \mathcal{P}_f is constant for a large range of ω , like white noise, and decays rapidly above a cut-off frequency (~ 10 Hz). For higher c , \mathcal{P}_f develops a peak with a characteristic frequency (3.8 ± 0.2 Hz), which differs from the inertial frequency of the system, $\omega_{\text{sys}} = \frac{1}{2\pi} \sqrt{\frac{k}{M}} = 7.6$ Hz.

We focus now on the system's transition from the *crackling* to *erratic* to *periodic*. Fig.3(a) shows the evolution of the PSD, \mathcal{P}_f for the force, as c varies, for fixed k [44]. Considering the crackling regime (small c) and ignoring the flat part of the curve for very high frequencies (corresponding with sensor limit) \mathcal{P}_f can be fitted

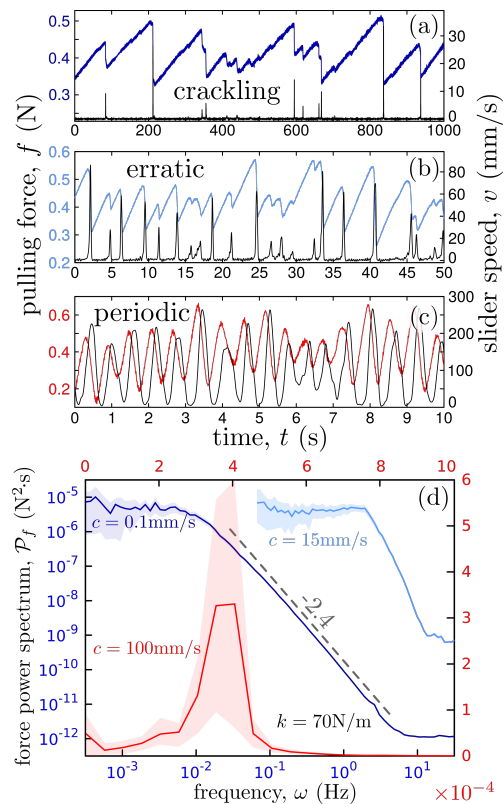


FIG. 2. (color online) Typical signals. Evolution of the slider speed $v(t)$ (black) and pulling force $f(t)$ (colored) for different loading speeds ($c = 0.1, 15$ and 100 mm/s) displaying different dynamics: crackling at low speed (a), erratic at medium speed (b) and periodic at high speed (c). (d): Corresponding power spectral density (PSD) of the force signal \mathcal{P}_f . A dashed line shows a slope corresponding with the exponent -2.4 ± 0.2 fitted on the power-law obtained for $c = 0.1$ mm/s. The shaded area shows the 95% confidence interval of the curves. The blue curves are in log-log space. Experiments are carried out with a spring of stiffness $k = 192$ N/m.

to a gamma-law: $\mathcal{P}_f(\omega) \propto (1 + \omega/\omega_{\text{min}})^{-\beta} e^{-\omega/\omega_{\text{max}}}$, where ω_{min} and ω_{max} are the lower and upper power-law cut-offs respectively, and $\beta = 2.4 \pm 0.2$. The number of decades for which \mathcal{P}_f obeys a power-law, $\log_{10}(\omega_{\text{max}}) - \log_{10}(\omega_{\text{min}})$, decreases as c increases. This is quantified in the inset of fig.3(b), showing that the number of power-law decades is roughly inversely proportional to the loading speed: $\omega_{\text{max}}/\omega_{\text{min}} \propto 1/c$. Moreover, in the inset of fig.3(a), all \mathcal{P}_f curves, except for their upper cut-offs, collapse when ω is scaled by the loading speed, c . This collapse implies that $\omega_{\text{min}} = \kappa c$, where κ is a characteristic wave number depending on the system's stiffness, pressure and geometry, but not c . For higher loading speeds, a bump appears close to ω_{min} . The appearance of this peak indicates the onset of oscillations at a frequency ω_c . The inset of fig.3(a) shows that, unlike ω_{min} , ω_c does not scale with c , since the peaks do not collapse. Fig.3(b) shows that the value of \mathcal{P}_f at the peak

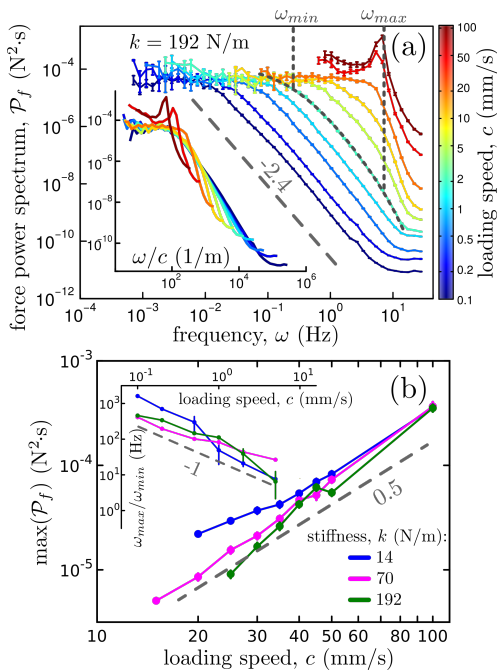


FIG. 3. (color online) (a): Force power spectra $\mathcal{P}_f(\omega)$ for different loading speeds, $c \in [0.1, 100]$ mm/s with $k = 192$ N/m. For $c = 2$ mm/s, \mathcal{P}_f is fitted by a gamma function displayed by a dashed line with lower (ω_{min}) and upper (ω_{max}) cut-off positions. A straight dashed line shows a slope corresponding with the exponent -2.4 fitted for the lowest c curve. Inset: \mathcal{P}_f with the frequency scaled by c . (b) Maximum of \mathcal{P}_f as a function of c , for power spectra with a bump. A dashed line with slope 0.5 is given to guide the eye. Inset: Spreading of the power-law regime (if any) $\omega_{max}/\omega_{min}$ as a function of c . A dashed line with slope -1 is given to guide the eye. Different curves correspond to different stiffnesses, k .

is sub-linear in c , with an exponent close to 0.5. This scaling quantifies the strength of the oscillations.

Fig.4a presents a phase diagram as a function of the two parameters that quantify crackling and periodicity, namely, the loading speed, c , and the system stiffness, k . The number of decades ($\log_{10} \omega_{max}/\omega_{min}$) is higher for lower loading speeds and stiffnesses. This is the domain where the crackling regime is dominant. Conversely, the value of \mathcal{P}_f at the peak is higher for higher c and k . This is the domain where the periodic regime is dominant. Between, where both former quantities, power-law spanning and peak, vanish or cannot be measured, lies the erratic regime. This is a continuous transition and we do not detect a critical loading speed between crackling and periodic behavior. The crackling and erratic and erratic and periodic regimes coexist with the dominant behavior depending on c and k values. Fig.4b shows how the oscillation frequency changes as a function of c for three different k 's. We observe a logarithmic dependence, $\omega_c \propto \log c$. This relation is consistent with a homoclinic bifurcation with c as the bifurcation parameter[45]. Furthermore, the curves for different stiffnesses collapse on

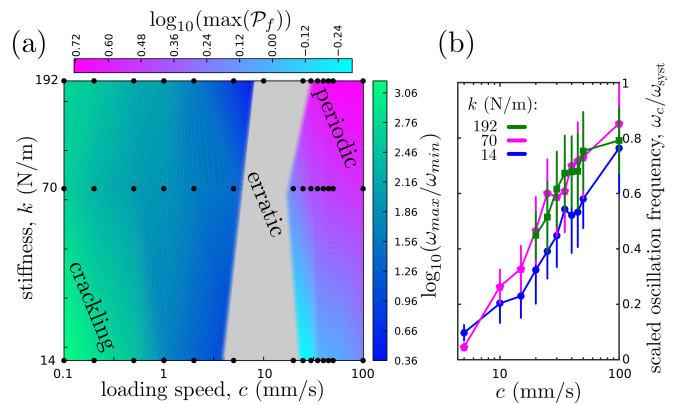


FIG. 4. (color online) (a) Phase diagram of dynamics: Map of the maximum of \mathcal{P}_f for PSD out of the power-law regime (right) and of the power-law spreading (if any) $\omega_{max}/\omega_{min}$ (left) as a function of the loading speed c and the system stiffness k . High \mathcal{P}_f corresponds to periodic regime while high $\omega_{max}/\omega_{min}$ corresponds to crackling regime. The middle transition area in gray corresponds to erratic dynamics. Black dots are experimental measurement points, and the rest of the map is linearly extrapolated (in the log space). (b) Evolution of PSD peak frequency, ω_c , scaled by ω_{sys} , as a function of c in log-lin scale. The logarithmic dependence, $\omega_c \propto \log c$, shows a homoclinic bifurcation for this transition. The scaling collapses the curves for different stiffnesses.

each other when ω_c is scaled by $\omega_{sys} = (k/M)^{1/2}$ [46]. We cannot distinguish the bifurcation critical speed, c_0 , from zero. It is possible that the bifurcation occurs at $c = 0$ and there is periodicity all over the phase space of c and k . However, we cannot detect the periodic behavior for lower c due to small amplitude and frequency of oscillations.

We also investigate the force signal probability distribution function (PDF), $P(f)$. Fig.5(a) shows $P(f)$ for different c , and fixed k . Regardless of the shear rate, these PDF's are well fitted by a Gaussian function of standard deviation $\sigma(c, k)$. We note that the mean value of the shear stress is independent of the loading speed in the range of speeds explored in these experiments. Similarly, as shown in the upper inset of fig.5(a), the fluctuations of the force signal, quantified by σ , remain constant ($\sigma \approx 0.065$) in the crackling and erratic regimes. However, σ starts to increase when the periodic behavior is first observed (from $c \approx 20$ mm/s).

We have also explored the effect of other macroscopic parameters. Unlike previous findings [38], changing the depth of the granular layer, L , does not change the system's behavior [47] to our experimental precision. The granular shear creates a narrow shear band, which induces a flow limited to the few top layers of grains. The narrowness of this shear band, in which all the plastic granular flow occurs, is likely responsible for the fact that L does not play a significant role in our experiment. However, the granular global pressure, from the slider

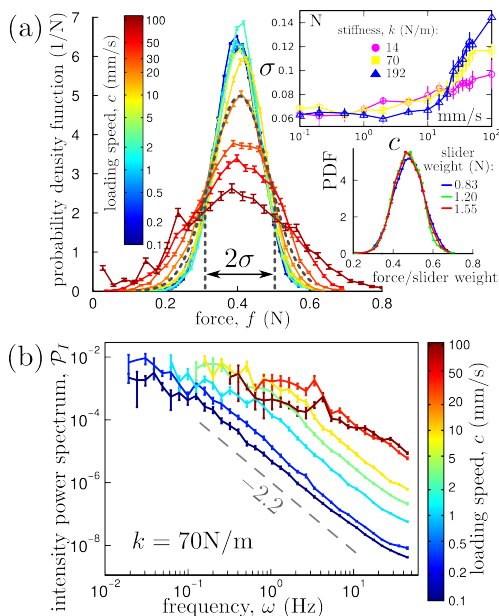


FIG. 5. (color online) (a) Probability density function (PDF) of force $P(f)$, for different loading speeds, c , at fixed stiffness $k = 192 \text{ N/m}$. For $c = 20 \text{ mm/s}$, $P(f)$ is fitted by a Gaussian displayed by a dashed line, enlightening the standard deviation σ . Inset-up: σ vs. c for different stiffnesses, $k \in \{14, 70, 192\} \text{ N/m}$. Inset-down: PDF of the force signal scaled by the slider weight (in N) for different weights, $Mg \in \{0.83, 1.2, 1.55\} \text{ N}$. The loading speed is $c = 0.5 \text{ mm/s}$ and the stiffness is $k = 192 \text{ N/m}$. (b) Image intensity ($I(t)$) power spectra $\mathcal{P}_I(\omega)$ for different loading speeds $c \in [0.1, 100] \text{ mm/s}$ with $k = 70 \text{ N/m}$. A straight dashed line shows a slope corresponding with the exponent -2.2 ± 0.2 fitted to the lowest speed.

weight, Mg , changes the force PDF's significantly. The lower inset of fig.5(a) shows these PDF's scaled by the slider mass, f/M . $P(f)$ for different M collapse on a single Gaussian curve which indicates the slider weight controls both the mean and fluctuations of f [48]. This collapse also implies a linear relation between the global pressure, P , and the mean granular shear stress acting on the slider, τ , and the shear stress fluctuations σ_τ . This linear relation provides a well-defined and constant average friction coefficient, $\mu = \bar{\tau}/P$, for our slowly sheared granular medium.

We next consider the relation between the global dynamics, as characterized by the force signal, and the local dynamics determined by the stress inside the granular bed. The grain-scale stress is computed from the polarized image intensities I [49]. Fig.5(b) shows the image intensity PSD \mathcal{P}_I as a function of c at fixed k . Like \mathcal{P}_f in the crackling regime, \mathcal{P}_I follows a power-law with exponent -2.2 ± 0.2 , and the frequency interval of this power-law regime decreases as c increases. However, we do not observe a clear peak in \mathcal{P}_I , indicative of a periodic regime, as c increases. We believe this is due to the differ-

ences in particle's inertia and stiffness compared to those of the slider and the spring. Specifically, the granular material is significantly stiffer than the spring, and it has a lower mass. For high c , these differences result in interior granular fluctuations that are much faster than the global fluctuations associated with the slider and spring [50]. These granular stress fluctuations, which exhibit the effective friction on the slider, looks almost the same for different loading speeds. Consequently, the global periodic oscillations are not directly caused by the underlying granular friction, rather it is due to the coupling with an external spring. This is also consistent with the fact that we do not observe a periodic regime as $k \rightarrow \infty$ [51].

Concluding discussion – The experiments reported here demonstrate that different behaviors, namely crackling, erratic and periodic dynamics, occur in sheared granular media, depending on the shear rate and system stiffness, without a sharp crossovers between different regimes. The other main observations of these experiments are: (i) The shearing force PSD provides a useful tool to indicate which regime is dominant for a given set of system control parameters, namely loading speed, system's stiffness, global pressure, and system size. (ii) The transition to periodic regime is similar to a homoclinic bifurcation, where c is the the primary control parameter. (iii) The shearing force PDF follows a Gaussian distribution with a standard deviation, σ , that bifurcates at the onset of periodicity; σ is nearly independent of c below the periodic regime, and grows sharply with c above the transition. (iv) No clear periodicity is observed for the local dynamics, including when the slider is in the periodic regime.

These observations are in agreement with various numerical simulations. Lacombe et al. [40] introduced a simple friction model, similar to our experiment, with a two dimensional propagation equation containing a friction kernel. They reproduced stick-slip, inertial oscillations and sliding regimes by increasing the shear rate. However, no crackling dynamics was observed, since their model does not contain explicit stochastic driving. Our phase diagram, presented in fig.4, may be a detailed version of the stick-slip domain of their diagram. In an experimental study, Kaproth et al. [34] observed only periodic stick-slip and sliding regimes, and the driving rate only affects the slip event period. We believe they do not observe crackling dynamics because of mono-dispersivity of their granular layers. In other studies, Aharonov et al. [37] simulated a system very similar to ours using the discrete element method (DEM). They also observed crackling, oscillatory and sliding regimes by changing the loading speed and the slider mass. However, the effect of the stiffness was not tested and the exact domain of the crackling regime were not investigated. Liu et al. [38] also studied the effect of the driving rate on avalanches. As in our experiments, they observed that increasing the driving rate decreases the power-law range of the avalanche size distribution, i.e. the number of decades

over which the avalanche size PDF obeys a power-law. Avalanches have also been observed in depinning models and a phase diagram of dynamical regimes for such a model has been demonstrated [52] as a function of c , k and L .

The findings of this letter can inform a number of open problems, ranging from avalanche dynamics for non-zero shear rate in many systems, to rheology of the sheared granular media, fracture dynamics and the depinning transition. Future work at higher loading speeds is required to fully investigate the periodic to steady sliding transition and to understand global and local (space-time) avalanche statistics in the crackling regime.

Acknowledgements: We would like to acknowledge Sid Nagel, Josh Socolar, and Stephen Teitworth for their helpful conversations and funding supports from NSF-DMR1206351, NASA NNX15AD38G, The William M. Keck Foundation and DARPA grant 4-34728.

* aghil.abed.zadeh@duke.edu

† jb@jonathan-bares.eu

- [1] I. Regev, J. Weber, C. Reichhardt, K. A. Dahmen, and T. Lookman. Reversibility and criticality in amorphous solids. *Nature communications*, 6, 2015.
- [2] J. Lin, T. Gueudré, A. Rosso, and M. Wyart. Criticality in the approach to failure in amorphous solids. *Physical review letters*, 115(16):168001, 2015.
- [3] C. E. Maloney and A. Lemaitre. Amorphous systems in athermal, quasistatic shear. *Physical Review E*, 74(1):016118, 2006.
- [4] P. Bak, K. Christensen, L. Danon, and T. Scanlon. Unified scaling law for earthquakes. *Physical Review Letter*, 88(17):178501, Apr 2002.
- [5] J. Davidsen and G. Kwiatek. Earthquake interevent time distribution for induced micro-, nano-, and picoseismicity. *Physical review letters*, 110(6):068501, 2013.
- [6] M. J. Alava, P. K. V. V. Nukala, and S. Zapperi. Statistical models of fracture. *Advances in Physics*, 55(3-4):349–476, 2006.
- [7] D. Bonamy, S. Santucci, and L. Ponson. Crackling dynamics in material failure as the signature of a self-organized dynamic phase transition. *Physical Review Letters*, 101(4):045501, Jul 2008.
- [8] J. Barés, M. L. Hattali, D. Dalmas, and D. Bonamy. Fluctuations of global energy release and crackling in nominally brittle heterogeneous fracture. *Physical Review Letters*, 2014.
- [9] A. Petri, G. Paparo, A. Vespignani, A. Alippi, and M. Costantini. Experimental evidence for critical dynamics in microfracturing processes. *Physical Review Letters*, 73(25):3423, 1994.
- [10] H. V. Ribeiro, L. S. Costa, L. G. A. Alves, P. A. Santoro, S. Picoli, E. K. Lenzi, and R. S. Mendes. Analogies between the cracking noise of ethanol-dampened charcoal and earthquakes. *Physical review letters*, 115(2):025503, 2015.
- [11] W. F. Brace and J. D. Byerlee. Stick-slip as a mechanism for earthquakes. *Science*, 153(3739):990–992, 1966.
- [12] P. A. Johnson, H. Savage, M. Knuth, J. Gomberg, and C. Marone. Effects of acoustic waves on stick-slip in granular media and implications for earthquakes. *Nature*, 451(7174):57–60, 2008.
- [13] S. Zapperi, A. Vespignani, and H. E. Stanley. Plasticity and avalanche behaviour in microfracturing phenomena. *Nature*, 388(6643):658, 1997.
- [14] S. Papanikolaou, D. M. Dimiduk, W. Choi, J. P. Sethna, M. D. Uchic, C. F. Woodward, and S. Zapperi. Quasi-periodic events in crystal plasticity and the self-organized avalanche oscillator. *Nature*, 490(517), 2012.
- [15] J. S. Urbach, R. C. Madison, and J. T. Markert. Interface depinning, self-organized criticality, and the barkhausen effect. *Physical Review Letters*, 75:276–279, 1995.
- [16] G. Durin and S. Zapperi. The barkhausen effect. In G. Bertotto and I. Mayergoyz, editors, *The Science of Hysteresis*, page 181. Academic, New York, 2005.
- [17] D. Ertaş and M. Kardar. Critical dynamics of contact line depinning. *Physical Review E*, 49(4):R2532, 1994.
- [18] R. Planet, S. Santucci, and J. Ortín. Avalanches and non-gaussian fluctuations of the global velocity of imbibition fronts. *Phys. Rev. Lett.*, 102:094502, Mar 2009.
- [19] J. M. Beggs and D. Plenz. Neuronal avalanches in neocortical circuits. *Journal of neuroscience*, 23(35):11167–11177, 2003.
- [20] T. Bellay, A. Klaus, S. Seshadri, and D. Plenz. Irregular spiking of pyramidal neurons organizes as scale-invariant neuronal avalanches in the awake state. *Elife*, 4:e07224, 2015.
- [21] B. Miller, Corey C. O’Hern, and R. P. Behringer. Stress fluctuations for continuously sheared granular materials. *Physical Review Letters*, 77(15):3110, 1996.
- [22] N. W. Hayman, L. Ducloué, K. L. Foco, and K. E. Daniels. Granular controls on periodicity of stick-slip events: Kinematics and force-chains in an experimental fault. *Pure and Applied Geophysics*, 168(12):2239–2257, 2011.
- [23] S. P. Pudasaini and K. Hutter. *Avalanche dynamics: dynamics of rapid flows of dense granular avalanches*. Springer Science & Business Media, 2007.
- [24] A. Le Bouil, A. Amon, S. McNamara, and J. Crassous. Emergence of cooperativity in plasticity of soft glassy materials. *Physical Review Letters*, 112:246001, Jun 2014.
- [25] J. Barés, D. Wang, D. Wang, T. Bertrand, C. S. O’Hern, and R. P. Behringer. Local and global avalanches in a two-dimensional sheared granular medium. *Physical Review E*, 96:052902, Nov 2017.
- [26] J. P. Sethna, K. A. Dahmen, and C. R. Myers. Crackling noise. *Nature*, 410(6825):242–250, 2001.
- [27] D. Bi, J. Zhang, B. Chakraborty, and R. P. Behringer. Jamming by shear. *Nature*, 480(7377):355–358, 2011.
- [28] D. Howell, R. P. Behringer, and C. Veje. Stress fluctuations in a 2d granular couette experiment: A continuous transition. *Physical Review Letters*, 82:5241–5244, Jun 1999.
- [29] I. Albert, P. Tegzes, R. Albert, J. G. Sample, A.-L. Barabási, T. Vicsek, B. Kahng, and P. Schiffer. Stick-slip fluctuations in granular drag. *Physical Review E*, 64(3):031307, 2001.
- [30] A. Petri, A. Baldassarri, F. Dalton, G. Pontuale, L. Pietronero, and S. Zapperi. Stochastic dynamics of a sheared granular medium. *The European Physical Journal B*, 64(3-4):531–535, 2008.
- [31] S Lherminier, R Planet, G Simon, M Måløy, L Vanel,

- and O Ramos. A granular experiment approach to earthquakes. *Revista Cubana de Física*, 33(1):55–58, 2016.
- [32] S. Nasuno, A. Kudrolli, A. Bak, and J. P. Gollub. Time-resolved studies of stick-slip friction in sheared granular layers. *Physical Review E*, 58(2):2161, 1998.
- [33] S. Nasuno, A. Kudrolli, and J. P. Gollub. Friction in granular layers: Hysteresis and precursors. *Physical Review Letters*, 79(5):949, 1997.
- [34] B. M. Kaproth and C. Marone. Slow earthquakes, pre-seismic velocity changes, and the origin of slow frictional stick-slip. *Science*, 341(6151):1229–1232, 2013.
- [35] J. Krim, P. Yu, and R. P. Behringer. Stick-slip and the transition to steady sliding in a 2d granular medium and a fixed particle lattice. *Pure and applied geophysics*, 168(12):2259–2275, 2011.
- [36] K. A. Dahmen, Y. Ben-Zion, and J. T. Uhl. A simple analytic theory for the statistics of avalanches in sheared granular materials. *Nature Physics*, 7(7):554–557, 2011.
- [37] E. Aharonov and D. Sparks. Stick-slip motion in simulated granular layers. *Journal of Geophysical Research: Solid Earth*, 109(B9), 2004.
- [38] C. Liu, E. E. Ferrero, F. Puosi, J.-L. Barrat, and K. Martens. Driving rate dependence of avalanche statistics and shapes at the yielding transition. *Physical review letters*, 116(6):065501, 2016.
- [39] R. A. White and K. A. Dahmen. Driving rate effects on crackling noise. *Physical review letters*, 91(8):085702, 2003.
- [40] F. Lacombe, S. Zapperi, and H. J. Herrmann. Dilatancy and friction in sheared granular media. *The European Physical Journal E: Soft Matter and Biological Physics*, 2(2):181–189, 2000.
- [41] A. Abed Zadeh, J. Barés, and R. P. Behringer. Avalanches in a granular stick-slip experiment: detection using wavelets. *EPJ Web of Conference*, 140(03038), 2017.
- [42] see SM for a full picture of the experiment (Fig. S1).
- [43] A. Baldassarri, F. Dalton, A. Petri, S. Zapperi, G. Pontuale, and L. Pietronero. Brownian forces in sheared granular matter. *Physical review letters*, 96(11):118002, 2006.
- [44] see SM for curves of other k values (Fig. S2).
- [45] S. H. Strogatz. *Nonlinear dynamics and chaos: with applications to physics, biology, chemistry, and engineering*. Westview press, 2014.
- [46] see SM for unscaled curves (Fig. S3).
- [47] see SM for \mathcal{P}_f and $P(f)$ for different L (Fig. S5).
- [48] see SM for non-scaled curves (Fig. S4).
- [49] see SM for the calibration between $f(t)$ and $I(t)$ (Fig. S7).
- [50] see SM for a comparison between $f(t)$ and $I(t)$ signals for different loading speeds (Fig. S6).
- [51] see SM for $k = \infty$ PSD (Fig. S6).
- [52] J. Barés, L. Barbier, and D. Bonamy. Crackling versus continuumlike dynamics in brittle failure. *Physical review letters*, 111(5):054301, 2013.